

# Atomic, electronic, and magnetic structure of the Au(100)/Fe<sub>3</sub>O<sub>4</sub>(100) interface: Density functional theory study

Y. L. Li,<sup>1,\*</sup> K. L. Yao,<sup>1,2,†</sup> Q. H. Lu,<sup>1</sup> Z. L. Liu,<sup>1</sup> D. Xi,<sup>3</sup> X. P. Luo,<sup>3</sup> and Q. Ning<sup>3</sup>

<sup>1</sup>Department of Physics, Huazhong University of Science and Technology, Wuhan 430074, People's Republic of China

<sup>2</sup>International Center of Materials Physics, The Chinese Academy of Science, Shenyang 110015, People's Republic of China

<sup>3</sup>Tong ji Hospital, Huazhong University of Science and Technology, Wuhan 430074, People's Republic of China

(Received 21 November 2006; revised manuscript received 13 January 2007; published 17 April 2007)

The relative stability, the electronic structure, and the magnetic properties of the four models for Au(100)/Fe<sub>3</sub>O<sub>4</sub>(100) interface have been studied using density functional theory. From calculations, we find that all the interface energies of the four models are dependent linearly on the O chemical potential. At the same time, we predict the most stable structure of Au(100)/Fe<sub>3</sub>O<sub>4</sub>(100) interface. The density of states, the total energies, and the atomic spin magnetic moments of the four interface models are also calculated, which show that the half-metallic properties of bulk Fe<sub>3</sub>O<sub>4</sub> are destroyed in the four models due to the charge transfer between Au layers and the Fe<sub>3</sub>O<sub>4</sub> surface. In addition, from the total energies of the relaxed interface models in three magnetic states corresponding to ferromagnetic, antiferromagnetic, and nonmagnetic, we get the ground states of the four relaxed interface models, respectively.

DOI: 10.1103/PhysRevB.75.165314

PACS number(s): 71.15.Mb, 73.20.-r

## I. INTRODUCTION

The interface of transition-metal oxide and metal is receiving a lot of attention due to its technological applications in magnetic devices such as magnetic-field sensors, spin valves, read heads, and high-density magnetic recording media.<sup>1-8</sup> Among transition-metal oxide, half-metallic ferrimagnetic materials such as magnetite (Fe<sub>3</sub>O<sub>4</sub>) are of interest for use in spintronic devices, which exploit both the spin and charge of an electron in spin-dependent charge transport. Fe<sub>3</sub>O<sub>4</sub> has a cubic inverse-spinel structure at room temperature, where the O<sup>2-</sup> anions form a fcc lattice, one-third of the Fe ions (Fe<sup>3+</sup>) occupy the tetrahedral interstices (A sites), and the other two-thirds of the Fe ions (half Fe<sup>3+</sup> and half Fe<sup>2+</sup>) are located in the octahedral interstices (B sites).<sup>9</sup> Fe<sub>3</sub>O<sub>4</sub> has a relatively high transition temperature of 851 K.<sup>10</sup>

Epitaxial thin films of Fe<sub>3</sub>O<sub>4</sub> have been grown on the low-index planes of Au by electrodeposition. On Au(100) substrate, a (100) Fe<sub>3</sub>O<sub>4</sub> orientation is observed in experiment.<sup>11</sup> As viewed from the (100) face of the Fe<sub>3</sub>O<sub>4</sub> crystal, the bulk unit cell can be described by four pairs of alternating atomic sublayers, which are shifted in the plane of the layer with respect to each other. Within a pair, one sublayer is composed of the A-site Fe<sup>3+</sup> cations (A layer) and the other sublayer is composed of the B-site Fe<sup>3+</sup>, Fe<sup>2+</sup> cations, and O<sup>2-</sup> anions (B layer).<sup>9</sup> For bulk Fe<sub>3</sub>O<sub>4</sub>, the (100) surface is equivalent to the (001) surface, so they have the same structure. For Fe<sub>3</sub>O<sub>4</sub> (001) surface, a  $(\sqrt{2} \times \sqrt{2})R45^\circ$  reconstruction has been observed experimentally.<sup>12-16</sup> However, the structure of Fe<sub>3</sub>O<sub>4</sub>(100) surface is still under debate and there are many views on the (001) surface.<sup>17-20</sup> In this paper, we construct Au/Fe<sub>3</sub>O<sub>4</sub> interface using Au(100) slab on Fe<sub>3</sub>O<sub>4</sub>(100) surface with the  $(\sqrt{2} \times \sqrt{2})R45^\circ$  structure, which is only one out of the different possible atomic structures for the Fe<sub>3</sub>O<sub>4</sub>(100) surface. So the calculated results probably will not fit the interface of Au(100) slab on a Fe<sub>3</sub>O<sub>4</sub>(100) surface with other atomic structure.

The inverse-spinel structure of bulk Fe<sub>3</sub>O<sub>4</sub> and our chosen cell with a  $(\sqrt{2} \times \sqrt{2})R45^\circ$  periodicity for Fe<sub>3</sub>O<sub>4</sub>(100) surface

are shown in Fig. 1. On the other hand, in order to construct the Au(100)/Fe<sub>3</sub>O<sub>4</sub>(100) interface model, we build a  $(2 \times 2 \times 2)$  supercell of Au and also choose a cell with  $(\sqrt{2} \times \sqrt{2})R45^\circ$  periodicity for Au(100) surface, which are shown in Fig. 2. Based on the surface cells of Fe<sub>3</sub>O<sub>4</sub>(100) and Au(100), four models of the Au(100)/Fe<sub>3</sub>O<sub>4</sub>(100) interface emerge immediately: (1) Au-A/Fe<sub>3</sub>O<sub>4</sub>-A model: the Fe<sub>3</sub>O<sub>4</sub>(100) surface is terminated with Fe<sub>A</sub> atoms (A layer) and the outermost Au atom layer sits above the surface Fe<sub>A</sub> atoms of Fe<sub>3</sub>O<sub>4</sub>(100) slab. (2) Au-B/Fe<sub>3</sub>O<sub>4</sub>-A model: the Fe<sub>3</sub>O<sub>4</sub>(100) surface is terminated with Fe<sub>A</sub> atom (A layer) and the second Au atom layer sits above the surface Fe<sub>A</sub> atoms of Fe<sub>3</sub>O<sub>4</sub>(100) slab. (3) Au-A/Fe<sub>3</sub>O<sub>4</sub>-B model: the Fe<sub>3</sub>O<sub>4</sub>(100) surface is terminated with Fe<sub>B</sub> and O atoms (B layer) and the outermost Au atom layer sits above the Fe<sub>A</sub> atoms in the second layer of Fe<sub>3</sub>O<sub>4</sub>(100) slab. (4) Au-B/Fe<sub>3</sub>O<sub>4</sub>-B model: the Fe<sub>3</sub>O<sub>4</sub>(100) surface is terminated with Fe<sub>B</sub> and O atoms (B layer) and the second Au atom layer sits above the Fe<sub>A</sub> atoms in the second layer of Fe<sub>3</sub>O<sub>4</sub>(100) slab. The stacking sequence of the four models

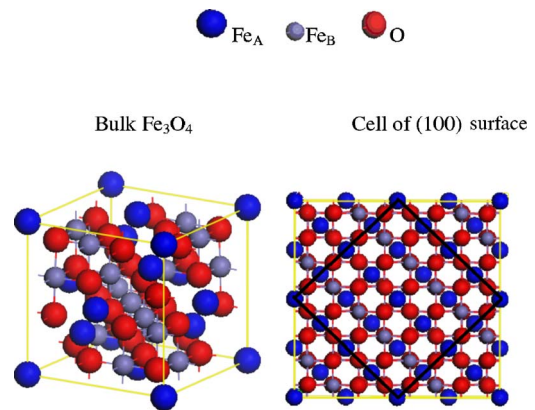


FIG. 1. (Color online) The inverse-spinel structure of magnetite together with the top view of the Fe<sub>3</sub>O<sub>4</sub>(100) surface unit cell with a  $(\sqrt{2} \times \sqrt{2})R45^\circ$  periodicity.

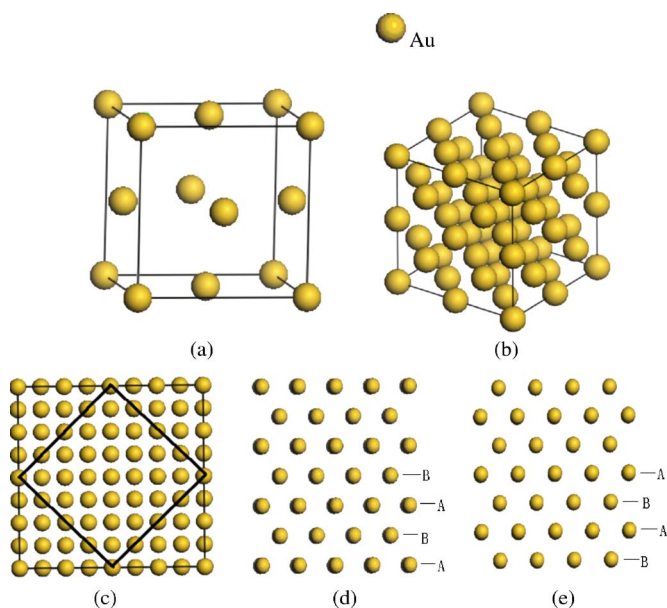


FIG. 2. (Color online) (a) The conventional cell of Au. (b) The  $(2 \times 2 \times 2)$  supercell of Au. (c) The top view of Au(100) surface unit cell with a  $(\sqrt{2} \times \sqrt{2})R45^\circ$  periodicity corresponding to  $(2 \times 2 \times 2)$  supercell. [(d) and (e)] The side view of Au(100) surface unit cell with a  $(\sqrt{2} \times \sqrt{2})R45^\circ$  periodicity corresponding to  $(2 \times 2 \times 2)$  supercell; thereinto (d) is the Au(100) surface terminated with A layer and (e) is the Au(100) surface terminated with B layer.

for Au(100)/Fe<sub>3</sub>O<sub>4</sub>(100) interface are shown in Fig. 3. To the best of our knowledge, so far, there is still little study on the property of Au(100)/Fe<sub>3</sub>O<sub>4</sub>(100) interface whether in theory or in experiment.

## II. METHODOLOGY

Our calculations are performed in the framework of density functional theory (DFT). We employ the full potential linearized augmented plane wave (FP-LAPW) method as implemented in the WIEN2K package<sup>21</sup> and the LDA+*U* calculations<sup>22</sup> with the self-interaction correction double-counting recipe for Fe<sub>3</sub>O<sub>4</sub> bulk, the Fe<sub>3</sub>O<sub>4</sub>(100) surface, and Au(100)/Fe<sub>3</sub>O<sub>4</sub>(100) interface, which is appropriate for strongly localized electrons. At the same time, the spin-orbit coupling is taken into account to supplement the local spin-density approximation results, which are applied to Fe atoms in the bulk, surface, and interface cells. In this LDA+*U* method, the strong correlation between localized *d* electrons is explicitly taken into account through the screened effective electron-electron interaction parameter  $U_{\text{eff}} = U - J$ , with *U*, and *J* denoting the Coulomb and exchange integrals, respectively.  $U_{\text{eff}}$  is an empirical parameter with the physical background of the Hubbard model. Usually, the Hubbard-type  $U_{\text{eff}}$  is evaluated by comparison of the theoretically calculated energy positions of energy bands with x-ray photoemission spectroscopy and ultraviolet photoemission spectroscopy measurements. However, the  $U_{\text{eff}}$  term is difficult to calculate accurately since it depends on the covalency of the system. Constrained calculations<sup>23</sup> with two types of charge

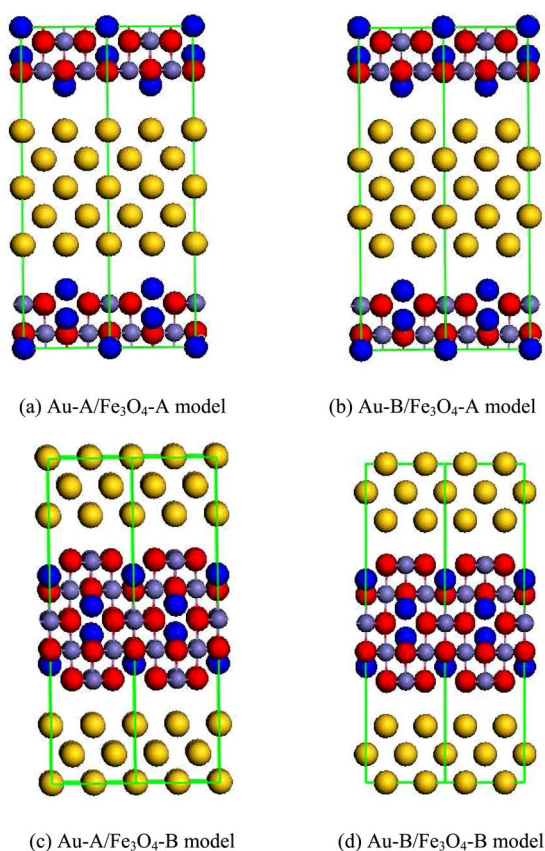


FIG. 3. (Color online) Structure of the Au(100)/Fe<sub>3</sub>O<sub>4</sub>(100) interface supercells in the perpendicular direction. The side view of the 9+5-layer supercell for the (a) Au-A/Fe<sub>3</sub>O<sub>4</sub>-A model, (b) Au-B/Fe<sub>3</sub>O<sub>4</sub>-A model, (c) Au-A/Fe<sub>3</sub>O<sub>4</sub>-B model, and (d) Au-B/Fe<sub>3</sub>O<sub>4</sub>-B model. Fe<sub>A</sub>, Fe<sub>B</sub>, and O atoms are marked by dark blue, light blue, and red circles.

ordering give  $U_{\text{eff}} = 4.5$  eV. The LDA+*U* band-structure calculations with  $U_{\text{eff}}$  varying from 4 to 6 eV provide optical, magneto-optical, and x-ray magnetic circular dichroism spectra in reasonable agreement with the experimental data. On the other hand, the value of the energy gap strongly depends on the value of  $U_{\text{eff}}$ . We have also justified the  $U_{\text{eff}}$  values within the FP-LAPW method for bulk Fe<sub>3</sub>O<sub>4</sub>.  $U_{\text{eff}}$  is set to 4.0 and 4.5 eV for the Fe<sub>B</sub> and Fe<sub>A</sub>, respectively. The results are in agreement with the previous theoretical results and experiments.<sup>24,25</sup>

In our calculations, the self-consistent-field calculations are based on the structural parameters: the atomic-sphere radii  $R_{\text{mt}}$  are chosen as 2.5, 2.0, and 1.6 a.u. for the Au, Fe, and O atoms, respectively. The cutoff parameter  $R_{\text{mt}}K_{\text{max}}$  for limiting the number of the plane waves is equal to 8.0, where  $K_{\text{max}}$  is the maximal value of the reciprocal lattice vector used in the plane-wave expansion and  $R_{\text{mt}}$  is the smallest atomic-sphere radius in the surface cell. So the plane-wave cutoff energy is 340 eV. In the atomic-sphere regions, the basis set consists of spherical harmonics with azimuthal quantum number  $l \leq 10$ , and nonspherical contributions of the charge density and potential with  $l \leq 5$ , and the potential was Fourier expanded up to  $G_{\text{max}} = 14$ . The *k* point mesh is chosen so that  $n_k = 8 \times 8 \times 6$  for the interfacial supercell,

TABLE I. Lattice constants of Au and Fe<sub>3</sub>O<sub>4</sub> observed in experiment and obtained from our calculations.

Lattice constant		Experiment (Å)	This work (Å)
Au	$a$	4.078	4.082
	$a'(2 \times 2 \times 2)$	8.157	8.164
	$\sqrt{2}a'$	11.534	11.544
Fe <sub>3</sub> O <sub>4</sub>	$a$	8.394	8.420
	$\sqrt{2}a$	11.869	11.906
Mismatch		2.9%	3.1%

which is used in this work. This set of parameters assures the total-energy convergence of 0.0001 Ry. The convergence was also checked by further increasing the cutoff energy and the  $k$ -point density. The atomic-sphere radii and the cutoff parameters of the four interfacial models are the same in our calculations.

### III. RESULTS AND DISCUSSION

Both Au and Fe<sub>3</sub>O<sub>4</sub> are cubic systems: the lattice constant of Fe<sub>3</sub>O<sub>4</sub> is 8.394 Å (Refs. 26 and 27) and that of Au(2 × 2 × 2) is 8.157 Å.<sup>28,29</sup> The lattice mismatch between bulk Au(2 × 2 × 2) and Fe<sub>3</sub>O<sub>4</sub> is 2.9%. The lattice constants of Au and Fe<sub>3</sub>O<sub>4</sub> observed in experiment and obtained from our optimized results have been listed in Table I.

As a first step to study the Au(100)/Fe<sub>3</sub>O<sub>4</sub>(100) interface, the properties of Au(100) and Fe<sub>3</sub>O<sub>4</sub>(100) surfaces were investigated from the thermodynamic side. Polar surfaces of compound materials have been the subject of intensive work in the past. Their orientation is such that each repeat unit in the direction perpendicular to the surface bears a nonzero dipole moment.<sup>30</sup>

To determine a reliable thickness for simulating a bulklike Au slab, we made systemic calculations for slabs of different thicknesses using the method proposed by Boettger<sup>31</sup> and Fiorentini *et al.*<sup>32</sup> As shown in Table II, the surface energy for the Au converges rapidly to 1.68 J/m<sup>2</sup> with increasing slab thickness, within about 0.01 J/m<sup>2</sup> for slabs with  $n \geq 5$ . So we chose five layers for the Au(100) slab. The same method was used for Fe<sub>3</sub>O<sub>4</sub>(100) slab, and we found that a slab consisting of 17 atomic layers was sufficient to converge the relaxation of the outermost five interlayer spacings. Then we chose 17 layers for the Fe<sub>3</sub>O<sub>4</sub>(100) slab. So based on the results of surface convergence tests, we constructed the Au(100)/Fe<sub>3</sub>O<sub>4</sub>(100) interface which has five layers for the Au(100) slab and 17 atomic layers for the Fe<sub>3</sub>O<sub>4</sub>(100) surface. We chose symmetric slabs for both Au and Fe<sub>3</sub>O<sub>4</sub>, and no vacuum region. This choice ensures zero net dipole moments, and hence, any unphysical dipole-dipole interactions between neighboring supercells are avoided.

Firstly, the total energies of the three magnetic states corresponding to ferromagnetic (FM), antiferromagnetic (AFM), and nonmagnetic (NM) for the four relaxed models have been given in Table III, from which we know that for

 TABLE II. Convergence of the Au(100) and Fe<sub>3</sub>O<sub>4</sub>(100) surface energies with respect to slab thickness.

Au(100) slab, $N$	Surface energy (J/m <sup>2</sup> )
3	1.73
5	1.68
7	1.69
9	1.70
11	1.68
Fe <sub>3</sub> O <sub>4</sub> (100) slab, $N$	Surface energy (J/m <sup>2</sup> )
3	8.47
5	8.56
7	9.09
9	9.33
11	9.38
13	9.06
15	9.47
17	9.68
19	9.65
21	9.67
23	9.68

the relaxed structures, Au-A/Fe<sub>3</sub>O<sub>4</sub>-A and Au-B/Fe<sub>3</sub>O<sub>4</sub>-A models have minimum total energies of −24 032.6582 and −24 035.4068 eV in AFM states, which shows that the main interactions are antiferromagnetic in the two models. In addition, we calculated the partial magnetic moment (MM), which have been listed in Table IV. The results reveal that there exist antiferromagnetic interactions between the atoms in the two interface cells and that the total magnetic moment of the interface cell is not equal to zero. So we conclude that the ferrimagnetic property of bulk Fe<sub>3</sub>O<sub>4</sub> remains in the relaxed Au-A/Fe<sub>3</sub>O<sub>4</sub>-A and Au-B/Fe<sub>3</sub>O<sub>4</sub>-A models and their ground states are ferromagnetic states. The energy difference  $\Delta E(AF\!M-F\!M)$  between AFM and FM is −2.093 and −0.313 eV for the relaxed Au-A/Fe<sub>3</sub>O<sub>4</sub>-A and Au-B/Fe<sub>3</sub>O<sub>4</sub>-A models, respectively. For the relaxed Au-A/Fe<sub>3</sub>O<sub>4</sub>-B and Au-B/Fe<sub>3</sub>O<sub>4</sub>-B models, they have minimum total energies in FM states, which are −24 034.5268 and −24 035.6677 eV, so FM states are their stable ground states. The energy difference  $\Delta E(AF\!M-F\!M)$  between AFM and FM is 1.042 and 0.152 eV for the relaxed Au-A/Fe<sub>3</sub>O<sub>4</sub>-B and Au-B/Fe<sub>3</sub>O<sub>4</sub>-B models, respectively. The ferrimagnetic property of bulk Fe<sub>3</sub>O<sub>4</sub> is destroyed in the

TABLE III. Total energies of three magnetic states in eV for the cell of the four relaxed interface models.

Model	FM	AFM	NM
Au-A/Fe <sub>3</sub> O <sub>4</sub> -A	−24030.5648	−24032.6582	−24028.0635
Au-B/Fe <sub>3</sub> O <sub>4</sub> -A	−24035.0937	−24035.4068	−24034.2361
Au-A/Fe <sub>3</sub> O <sub>4</sub> -B	−24034.5268	−24033.4847	−24032.7157
Au-B/Fe <sub>3</sub> O <sub>4</sub> -B	−24035.6677	−24035.5159	−24034.0916

TABLE IV. Calculated partial magnetic moments for Au(100)/Fe<sub>3</sub>O<sub>4</sub>(100) interface in the ideal and relaxed structures using the four models. The interface is marked by thick and dark lines.

Au-A/Fe <sub>3</sub> O <sub>4</sub> -A				Au-B/Fe <sub>3</sub> O <sub>4</sub> -A			
Layer	Element	Moment cal ( $\mu_B$ )		Layer	Element	Moment cal ( $\mu_B$ )	
		Ideal	Relaxed			Ideal	Relaxed
5	Au	-0.006	-0.308	5	Au	-0.010	-0.007
4	Au	0.011	-0.333	4	Au	0.016	-0.006
3	Au	-0.007	-0.347	3	Au	-0.015	-0.004
2	Au	0.004	-0.343	2	Au	0.014	-0.011
1	Au	-0.009	-0.299	1	Au	-0.013	0.026
1	Fe <sub>A</sub>	3.126	2.871	1	Fe <sub>A</sub>	3.547	3.527
2	O	0.211	0.789	2	O	0.345	0.325
	Fe <sub>B</sub>	-3.206	-2.959		Fe <sub>B</sub>	-3.955	-3.946
3	Fe <sub>A</sub>	3.362	3.150	3	Fe <sub>A</sub>	4.033	3.951
4	O	0.292	0.834	4	O	0.347	0.380
	Fe <sub>B</sub>	-3.211	-3.024		Fe <sub>B</sub>	-4.041	-3.984
5	Fe <sub>A</sub>	3.654	3.554	5	Fe <sub>A</sub>	4.051	3.531
6	O	0.275	0.960	6	O	0.359	0.342
	Fe <sub>B</sub>	-3.847	-3.782		Fe <sub>B</sub>	-4.061	-3.800
Au-A/Fe <sub>3</sub> O <sub>4</sub> -B				Au-B/Fe <sub>3</sub> O <sub>4</sub> -B			
Layer	Element	Moment cal ( $\mu_B$ )		Layer	Element	Moment cal ( $\mu_B$ )	
		Ideal	Relaxed			Ideal	Relaxed
5	Au	-0.001	-0.004	5	Au	-0.000	0.031
4	Au	0.002	-0.008	4	Au	-0.001	-0.002
3	Au	-0.000	-0.003	3	Au	-0.001	0.010
2	Au	0.008	-0.007	2	Au	-0.003	-0.011
1	Au	-0.001	-0.002	1	Au	-0.006	-0.005
1	O	0.417	0.384	1	O	0.423	0.377
	Fe <sub>B</sub>	-4.108	-4.063		Fe <sub>B</sub>	-4.123	-4.073
2	Fe <sub>A</sub>	4.124	4.057	2	Fe <sub>A</sub>	4.152	4.059
3	O	0.346	0.322	3	O	0.344	0.338
	Fe <sub>B</sub>	-4.068	-4.067		Fe <sub>B</sub>	-4.107	-4.060
4	Fe <sub>A</sub>	4.039	4.024	4	Fe <sub>A</sub>	4.095	4.040
5	O	0.247	0.226	5	O	0.286	0.246
	Fe <sub>B</sub>	-4.079	-3.814		Fe <sub>B</sub>	-4.093	-3.832
6	Fe <sub>A</sub>	3.576	3.545	6	Fe <sub>A</sub>	3.570	3.502

two relaxed models. At the same time, we have calculated the relaxation energy of the four relaxed structures. We find that the relaxed Au-A/Fe<sub>3</sub>O<sub>4</sub>-B and Au-B/Fe<sub>3</sub>O<sub>4</sub>-B models have relatively higher relaxation energies, 167.139 and 171.678 meV/Å<sup>2</sup>, respectively, which shows that the two relaxed models have larger change in structures after relaxation. The relaxation energy of Au-A/Fe<sub>3</sub>O<sub>4</sub>-A models are found to be the smallest (53.265 meV/Å<sup>2</sup>), which indicates that the Au-A/Fe<sub>3</sub>O<sub>4</sub>-A interface structures is the most rigid. The relaxation energy of Au-B/Fe<sub>3</sub>O<sub>4</sub>-A model is 83.963 meV/Å<sup>2</sup>, which is slightly larger than the Au-A/Fe<sub>3</sub>O<sub>4</sub>-A model.

Bulk Fe<sub>3</sub>O<sub>4</sub> is a ferrimagnet with the MM of tetrahedral Fe<sub>A</sub> (-3.43μ<sub>B</sub>) and octahedral Fe<sub>B</sub> (3.50μ<sub>B</sub>) oriented antiparallel to each other and a total MM of 4.0 μ<sub>B</sub>/f.u.<sup>17</sup> The main features of the partial MM in Table IV are as follows: (1) The MM of the interfacial Fe<sub>A</sub>, Fe<sub>B</sub>, and O atoms are substantially reduced in the relaxed models compared with the ideal models due to the strong relaxations. (2) For the relaxed Au-A/Fe<sub>3</sub>O<sub>4</sub>-A models, the MM of the interfacial Fe<sub>A</sub> atoms are smaller than the bulk value (-3.43μ<sub>B</sub>), while for the relaxed Au-B/Fe<sub>3</sub>O<sub>4</sub>-A models, the MM of the interfacial Fe<sub>A</sub> atoms are larger than the bulk value (-3.43μ<sub>B</sub>). (3) For the relaxed Au-A/Fe<sub>3</sub>O<sub>4</sub>-B and Au-B/Fe<sub>3</sub>O<sub>4</sub>-B models,

TABLE V. Interlayer distance of the four models perpendicular to the interface by relaxed calculation, in terms of absolute distance (Å) and as a percentage of the respective bulk spacing (shown in parentheses); positive for increase and negative for decrease.

Interlayer	Model	
	Au-A/Fe <sub>3</sub> O <sub>4</sub> -A (Relaxation)	Au-B/Fe <sub>3</sub> O <sub>4</sub> -A (Relaxation)
Au23	2.059 (0.9%)	2.011 (-1.4%)
Au12	2.078 (1.9%)	2.106 (3.2%)
Inter	2.527	2.231
Fe <sub>3</sub> O <sub>4</sub> 12	1.090 (3.8%)	0.930 (-11.4%)
Fe <sub>3</sub> O <sub>4</sub> 23	1.008 (-0.2%)	0.667 (-34.0%)
Fe <sub>3</sub> O <sub>4</sub> 34	1.090 (3.8%)	1.059 (0.8%)
Fe <sub>3</sub> O <sub>4</sub> 45	1.008 (-0.2%)	1.197 (18.5%)

Interlayer	Model	
	Au-A/Fe <sub>3</sub> O <sub>4</sub> -B (Relaxation)	Au-B/Fe <sub>3</sub> O <sub>4</sub> -B (Relaxation)
Au23	1.962 (-3.8%)	2.078 (1.9%)
Au12	2.026 (-0.7%)	2.029 (-0.5%)
Inter	1.806	2.286
Fe <sub>3</sub> O <sub>4</sub> 12	0.665 (-34.2%)	0.723 (-28.4%)
Fe <sub>3</sub> O <sub>4</sub> 23	1.133 (7.9%)	1.074 (2.3%)
Fe <sub>3</sub> O <sub>4</sub> 34	1.294 (28.1%)	1.252 (24.0%)
Fe <sub>3</sub> O <sub>4</sub> 45	0.688 (-34.5%)	0.665 (-36.7%)

the MM of the interfacial Fe<sub>B</sub> atoms are larger than the bulk value ( $3.50\mu_B$ ). (4) The interactions between interfacial Au and Fe<sub>A</sub> or O atoms induce the smaller MM of Au atoms in the four relaxed models.

In our considered four models for Au(100)/Fe<sub>3</sub>O<sub>4</sub>(100) interface, the atomic positions in the supercell were fully relaxed and optimized. The optimized interlayer distance of the four models perpendicular to the interface has been given in Table V. Some features are found in the perpendicular relaxations of the interfacial distance for the four models. The Au-A/Fe<sub>3</sub>O<sub>4</sub>-B model has the shortest interfacial separation of 1.806 Å, while the Au-A/Fe<sub>3</sub>O<sub>4</sub>-A model has the largest value of 2.527 Å. The interfacial distance of the other two models is intermediate to the two extremes. For the Au-A/Fe<sub>3</sub>O<sub>4</sub>-A model, the distance of the outermost layer and the second layer for Fe<sub>3</sub>O<sub>4</sub>(100) slab increases to 1.090 Å and the magnitude of relaxation as a percentage of the corresponding bulk spacing is 3.8%. While for the other three models, the distance of the outermost layer and the second layer for Fe<sub>3</sub>O<sub>4</sub>(100) slab decreases, which is 0.930, 0.665, and 0.723 Å for Au-B/Fe<sub>3</sub>O<sub>4</sub>-A model, Au-A/Fe<sub>3</sub>O<sub>4</sub>-B model, and Au-B/Fe<sub>3</sub>O<sub>4</sub>-B model, respectively. On the other hand, we found that for the Au-A/Fe<sub>3</sub>O<sub>4</sub>-A model and the Au-B/Fe<sub>3</sub>O<sub>4</sub>-A model, the distance of the outermost layer and the second layer for Au(100) slab increases, which is 2.078 Å (1.9%) and 2.106 Å (3.2%). While that for the Au-B/Fe<sub>3</sub>O<sub>4</sub>-B model

TABLE VI. Calculations of the adhesion energies ( $W_{ad}$ ), the interfacial separations ( $d_o$ ) for the four relaxed Au(100)/Fe<sub>3</sub>O<sub>4</sub>(100) interface models, and percentage of the respective ideal spacing (shown in parentheses); positive for increase and negative for decrease.

Model	$d_o$ (Å)	$W_{ad}$ (J/m <sup>2</sup> )
Au-A/Fe <sub>3</sub> O <sub>4</sub> -A	2.527 (-13.4%)	3.06
Au-B/Fe <sub>3</sub> O <sub>4</sub> -A	2.231 (-23.6%)	3.16
Au-A/Fe <sub>3</sub> O <sub>4</sub> -B	1.806 (-43.2%)	3.94
Au-B/Fe <sub>3</sub> O <sub>4</sub> -B	2.286 (-28.1%)	3.90

and Au-B/Fe<sub>3</sub>O<sub>4</sub>-B model decreases, which is 2.026 Å (-0.7%) and 2.029 Å (-0.5%). Generally speaking, we find that the Au-A/Fe<sub>3</sub>O<sub>4</sub>-B model and Au-B/Fe<sub>3</sub>O<sub>4</sub>-B model have relatively larger change in structures by comparison of the relaxation percentage, which is consistent with the above analysis of the relaxation energy.

To assess the adhesive strength of the interfaces quantitatively, we have calculated the adhesion energy of Au(100)/Fe<sub>3</sub>O<sub>4</sub>(100) interface per unit area  $W_{ad}$  from

$$W_{ad} = (E_{Au}^{tot} + E_{Fe_3O_4}^{tot} - E_{Au/Fe_3O_4}^{tot})/A. \quad (1)$$

Here,  $E_{Au}^{tot}$  and  $E_{Fe_3O_4}^{tot}$  are the total energy of the relaxed, isolated Au and Fe<sub>3</sub>O<sub>4</sub> slabs in the same supercell when one of the slabs is retained and the other is replaced by vacuum, respectively.  $E_{Au/Fe_3O_4}^{tot}$  is the total energy of the Au(100)/Fe<sub>3</sub>O<sub>4</sub>(100) interface system.  $A$  is the interface area. Physically, the adhesion energy  $W_{ad}$  is the work per unit area required to separate the interface into two free surfaces within a microcanonical process, and it can be considered as a measure of the strength of the adhesion. Table VI shows the  $W_{ad}$  values and the interfacial separation  $d_0$  for the four interface structures. From Table VI, we can see that the relaxed Au-A/Fe<sub>3</sub>O<sub>4</sub>-B structure exhibits relatively larger adhesion energy (3.94 J/m<sup>2</sup>) and the shortest interfacial separation (1.806 Å), which decreases by 43.2% compared with the ideal Au-A/Fe<sub>3</sub>O<sub>4</sub>-B structure. So the interface of the Au-A/Fe<sub>3</sub>O<sub>4</sub>-B model tends to adhere strongly, which is related to the transfer of the compensating state from the Au(100) surface towards the interfacial O and Fe<sub>B</sub> atoms of Fe<sub>3</sub>O<sub>4</sub>(100) surface. The relaxed Au-A/Fe<sub>3</sub>O<sub>4</sub>-B structure is more stable than the other three models, while the relaxed Au-A/Fe<sub>3</sub>O<sub>4</sub>-A structure presents the smallest adhesion energy (3.06 J/m<sup>2</sup>), which shows that the Au-A/Fe<sub>3</sub>O<sub>4</sub>-A model is the least favorable structure.

In order to analyze the stability of the Au(100)/Fe<sub>3</sub>O<sub>4</sub>(100) interface structure, we give the interface energy  $\gamma$  according to the following formula:<sup>33</sup>

$$\gamma = (E_{interface} - N_{Fe}\mu_{Fe} - N_O\mu_O - N_{Au}\mu_{Au})/A - \sigma_{Au} - \sigma_{Fe_3O_4} \quad (2)$$

Here,  $E_{interface}$  is the total energy of the whole interface;  $\mu_{Fe}$ ,  $\mu_O$ , and  $\mu_{Au}$  are the chemical potentials of Fe, O, and Au, respectively. In addition,  $N_{Fe}$ ,  $N_O$ , and  $N_{Au}$  are the numbers

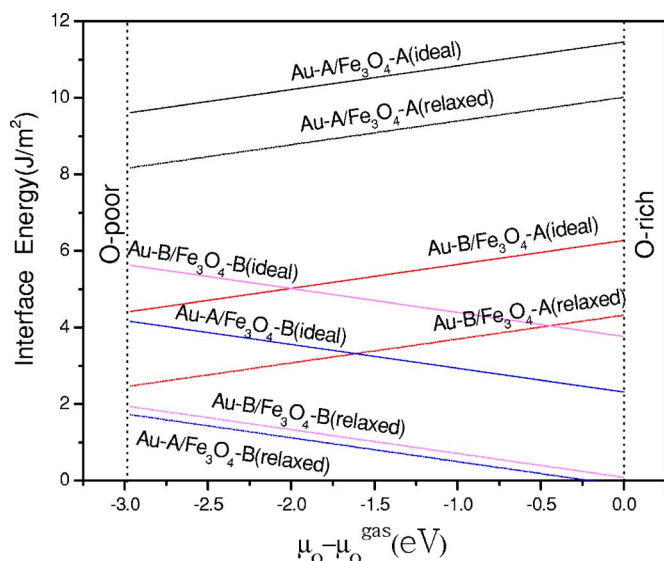


FIG. 4. (Color online) Interface energy for the four interfacial models as a function of  $\mu_{\text{O}} - \mu_{\text{O}}^{\text{gas}}$ .

of the corresponding atoms in the interface model.  $A$  is the area of the interface, and  $\sigma_{\text{Au}}$  and  $\sigma_{\text{Fe}_3\text{O}_4}$  are the surface energies of Au and  $\text{Fe}_3\text{O}_4$ , respectively. The total chemical potential of the Fe and O is in equilibrium with that of bulk  $\text{Fe}_3\text{O}_4$ :

$$3\mu_{\text{Fe}} + 4\mu_{\text{O}} = \mu_{\text{Fe}_3\text{O}_4(\text{bulk})}. \quad (3)$$

Accordingly, Eq. (2) becomes

$$\gamma = \{E_{\text{interface}} - (1/3)N_{\text{Fe}}\mu_{\text{Fe}_3\text{O}_4}(\text{bulk}) + [(4/3)N_{\text{Fe}} - N_{\text{O}}]\mu_{\text{O}} - N_{\text{Au}}\mu_{\text{Au}}\}/A - \sigma_{\text{Au}} - \sigma_{\text{Fe}_3\text{O}_4}. \quad (4)$$

The elemental Fe or O chemical potential must be less than the corresponding bulk and gas chemical potentials; otherwise, the element would form the energetically more favorable bulk structure. That is to say,

$$\mu_{\text{Fe}} \leq \mu_{\text{Fe}(\text{bulk})}, \quad \mu_{\text{O}} \leq \mu_{\text{O}(\text{gas})}. \quad (5)$$

Therefore, this  $\mu_{\text{O}}$  can be varied within certain boundaries. The lower boundary for  $\mu_{\text{O}}$ , which will be called the O-poor limit, is defined by the decomposition of the oxide into iron metal and oxygen. A reasonable upper boundary for  $\mu_{\text{O}}$ , on the other hand (O-rich limit), is given by gas phase conditions that are so oxygen rich that O condensation will start on the sample at low enough temperatures. Therefore, the range of the O chemical potential is<sup>34</sup>

$$\Delta H_f^0 \leq \mu_{\text{O}} - \mu_{\text{O}}^{\text{gas}} \leq 0, \quad (6)$$

where  $\Delta H_f^0 = (1/4)[\mu_{\text{Fe}_3\text{O}_4(\text{bulk})} - 3\mu_{\text{Fe}(\text{bulk})} - 4\mu_{\text{O}(\text{gas})}]$  is the 0 K heat of formation of bulk  $\text{Fe}_3\text{O}_4$ , which is taken to be  $-2.968$  eV. The O chemical potential is referenced with respect to the total energy of an oxygen molecule.  $\Delta\mu_{\text{O}} = \mu_{\text{O}} - \mu_{\text{O}}^{\text{gas}} = \mu_{\text{O}} - (1/2)E_{\text{O}_2}^{\text{total}}$ . The relationship of interface energy to the function of oxygen chemical potential  $\mu_{\text{O}} - \mu_{\text{O}}^{\text{gas}}$  is plotted in Fig. 4.

First, one can see that all the interface energies of the four models in ideal and relaxed structures depend linearly on  $\mu_{\text{O}} - \mu_{\text{O}}^{\text{gas}}$ . On the other hand, the interface energy of the relaxed structure is always lower than the corresponding ideal structure, which is evident in Fig. 4. Meanwhile, it is also found that the relaxed Au-A/ $\text{Fe}_3\text{O}_4$ -B interface model has the lowest interface energy and that the Au-A/ $\text{Fe}_3\text{O}_4$ -A model (ideal and relaxed) has the relatively higher interface energy over the whole oxygen chemical potential range. That is to say, the relaxed Au-A/ $\text{Fe}_3\text{O}_4$ -B structure appears to be more stable than other interface structures, while the Au-A/ $\text{Fe}_3\text{O}_4$ -A model is the most unstable structure, which is consistent with the above results of calculation.

Second, as the oxygen chemical potential increases, the interface energies increase for the Au-A/ $\text{Fe}_3\text{O}_4$ -A and Au-B/ $\text{Fe}_3\text{O}_4$ -A models, while the interface energies decrease for the Au-A/ $\text{Fe}_3\text{O}_4$ -B and Au-B/ $\text{Fe}_3\text{O}_4$ -B models. At the same time, we found that the relaxed Au-B/ $\text{Fe}_3\text{O}_4$ -A structure is more stable than the ideal Au-A/ $\text{Fe}_3\text{O}_4$ -B and Au-B/ $\text{Fe}_3\text{O}_4$ -B structures at the low oxygen chemical potential. However, as the oxygen chemical potential increases, the ideal Au-A/ $\text{Fe}_3\text{O}_4$ -B and Au-B/ $\text{Fe}_3\text{O}_4$ -B structures gradually become more stable.

Third, Table VI shows close adhesion energy for the relaxed Au-B/ $\text{Fe}_3\text{O}_4$ -A and Au-A/ $\text{Fe}_3\text{O}_4$ -A models, while Fig. 4 displays very different values of interface energy for the two models over the entire chemical potential range. As far as the reasons are concerned, we think perhaps that these are due to the relaxed Au-B/ $\text{Fe}_3\text{O}_4$ -A structure being able to continue the stacking sequence of  $\text{Fe}_3\text{O}_4(100)$  surface across the interface better than the relaxed Au-A/ $\text{Fe}_3\text{O}_4$ -A structure. The sequence of the Au-B/ $\text{Fe}_3\text{O}_4$ -A model in Fig. 3 is ABABA-B'A'B'A'B'-ABABA, while that of the Au-A/ $\text{Fe}_3\text{O}_4$ -A model is ABABA-A'B'A'B'A'-ABABA. So this preferred stacking sequence of the Au-B/ $\text{Fe}_3\text{O}_4$ -A model results in a relatively lower interface energy in Fig. 4.

In order to further characterize the interfacial electronic structure of the Au(100)/ $\text{Fe}_3\text{O}_4(100)$  interface, we also give the total density of states (DOS) of the interface models and the bulk  $\text{Fe}_3\text{O}_4$  in Fig. 5. Because the Au-A/ $\text{Fe}_3\text{O}_4$ -A model is the most unstable structure according to the above analysis, we discard that model and only discuss the other three models. As shown in Fig. 5, the plotted energy range is from  $-6$  to  $6$  eV for the bulk  $\text{Fe}_3\text{O}_4$  and from  $-8$  to  $8$  eV for the three interface models. Because the DOS distribution near the Fermi level determines the magnetic properties, we concentrate our attention on the DOS in the vicinity of the Fermi level, which is set to zero. From Fig. 5(a), we can see that the bulk  $\text{Fe}_3\text{O}_4$  shows a half-metallic behavior with a band gap in the majority-spin channel of approximately  $1.5$  eV and 100% spin polarization due to the  $t_{2g}$  states of  $\text{Fe}_B$  at  $E_F$  in the majority-spin channel.<sup>35</sup> Figures 5(b)–5(d) shows the total DOS of the ideal and relaxed structures for the three interface models, respectively. We notice that the total spin-up and spin-down DOS of the three relaxed structures are obviously split off and both of them cross the Fermi level, which shows that the half-metallic property is destroyed and all the three relaxed interface structures have metallic properties. Due to the interactions between the interfacial Au atom and the  $\text{Fe}_3\text{O}_4(100)$  surface, a large charge

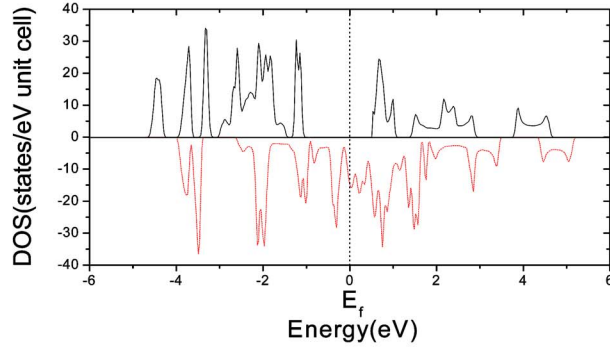
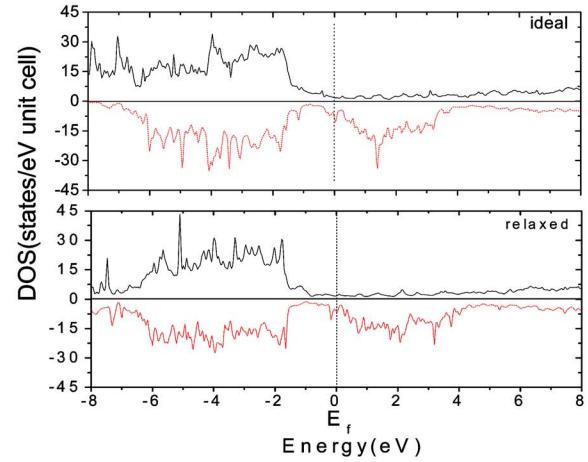
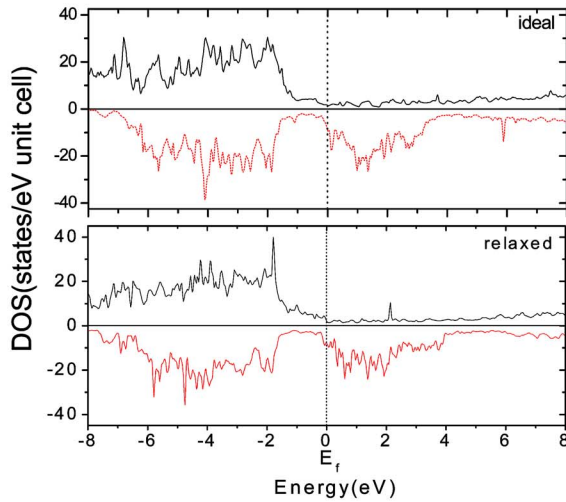
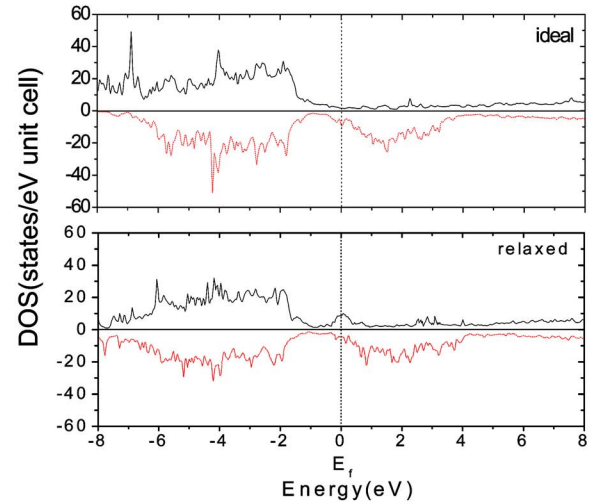

 (a) DOS of the bulk  $\text{Fe}_3\text{O}_4$ .

 (c) DOS of the Au-A/ $\text{Fe}_3\text{O}_4$ -B interface model.

 (b) DOS of the Au-B/ $\text{Fe}_3\text{O}_4$ -A interface model.

 (d) DOS of the Au-B/ $\text{Fe}_3\text{O}_4$ -B interface model.

FIG. 5. (Color online) Total density of states of (a) bulk  $\text{Fe}_3\text{O}_4$  and Au(100)/ $\text{Fe}_3\text{O}_4$ (100) interface, (b) Au-B/ $\text{Fe}_3\text{O}_4$ -A model, (c) Au-A/ $\text{Fe}_3\text{O}_4$ -B model, and (d) Au-B/ $\text{Fe}_3\text{O}_4$ -B model (solid lines, spin-up states; dashed lines, spin-down states; and dotted lines, the Fermi level).

transfer happens in the interface layer. Therefore all the three relaxed polar interfaces have metallic properties, which are different from the bulk  $\text{Fe}_3\text{O}_4$  properties. On the other hand, the DOS of the ideal and relaxed structures for the Au-B/ $\text{Fe}_3\text{O}_4$ -A model, the Au-A/ $\text{Fe}_3\text{O}_4$ -B model, and the Au-B/ $\text{Fe}_3\text{O}_4$ -B model have a similar character, which does not depend strongly on the absolute values of the interlayer relaxation. At the same time, we calculated the spin-polarization percentage  $P$  by the equation<sup>11</sup>

$$P = \frac{I(\uparrow) - I(\downarrow)}{I(\uparrow) + I(\downarrow)} \times 100\%, \quad (7)$$

where  $I(\uparrow)$  and  $I(\downarrow)$  are the measured intensities of spin-up and spin-down electrons, respectively. The values have been listed in Table VII. For the Au-B/ $\text{Fe}_3\text{O}_4$ -A model, the spin-

polarization percentage of the relaxed structure increases compared with that of the ideal structure, while for the Au-A/ $\text{Fe}_3\text{O}_4$ -B model, the spin-polarization percentage of the relaxed structure is smaller than that of the ideal structure. Even more interesting is that for the Au-B/ $\text{Fe}_3\text{O}_4$ -B model the spin-polarization percentage of the ideal structure is negative ( $-67.6\%$ ) and that of the relaxed structure is positive ( $22.4\%$ ), which is different from that of the other three models.

Figure 6 gives the layer-projected DOS of the three relaxed models. For the three models, all the DOS of interfacial Au  $d$  orbitals move to the low-energy states. For the relaxed Au-B/ $\text{Fe}_3\text{O}_4$ -A model, the interfacial  $\text{Fe}_A$ ,  $\text{Fe}_B$   $d$  orbitals and O  $p$  orbitals exhibit more occupied states at the Fermi level, arising from that of Au. For the relaxed Au-A/ $\text{Fe}_3\text{O}_4$ -B model, the DOS of the interfacial Au  $d$  or-

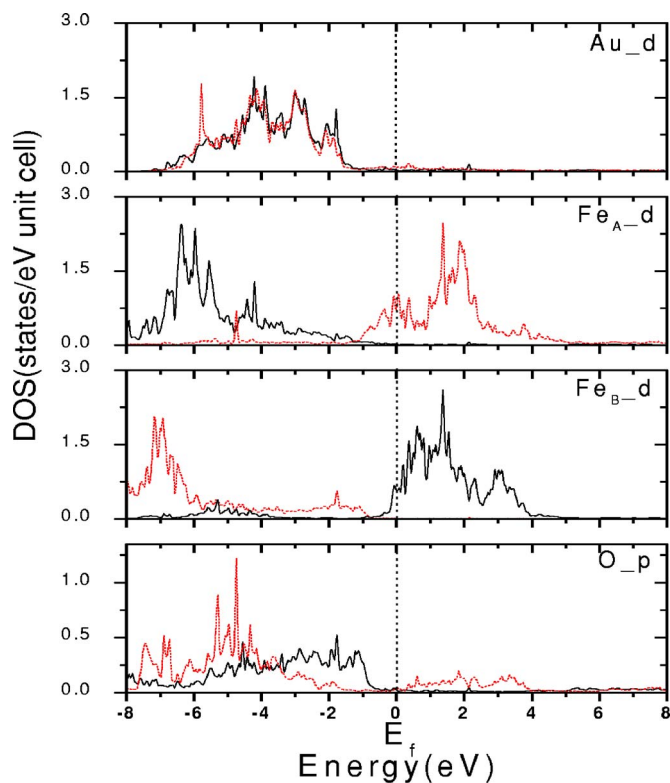
TABLE VII. Calculated results of the spin-polarization percentage  $P$  for Au(100)/Fe<sub>3</sub>O<sub>4</sub>(100) interface in the ideal and relaxed structures using the three models.

Model	Polarization percentage (%)
Au-B/Fe <sub>3</sub> O <sub>4</sub> -A (Ideal)	-71.0
Au-B/Fe <sub>3</sub> O <sub>4</sub> -A (Relaxed)	-75.2
Au-A/Fe <sub>3</sub> O <sub>4</sub> -B (Ideal)	-68.9
Au-A/Fe <sub>3</sub> O <sub>4</sub> -B (Relaxed)	-50.7
Au-B/Fe <sub>3</sub> O <sub>4</sub> -B (Ideal)	-67.6
Au-B/Fe <sub>3</sub> O <sub>4</sub> -B (Relaxed)	22.4

bitals and  $O p$  orbitals have more overlapping states at the range from  $-7$  to  $-1$  eV because of a considerable electron transfer across the interface. For the relaxed Au-B/Fe<sub>3</sub>O<sub>4</sub>-B model, the interfacial Au  $d$  orbitals and the  $O p$  orbitals have similar shape below the Fermi level. This shows the strong hybridization between the interfacial Au  $d$  and  $O p$  states.

#### IV. SUMMARY AND CONCLUSIONS

We have studied the four Au(100)/Fe<sub>3</sub>O<sub>4</sub>(100) interface models using DFT. The stability, the magnetic property, and the electronic structure of Au(100)/Fe<sub>3</sub>O<sub>4</sub>(100) interface have been calculated. The results show that the relaxed Au-A/Fe<sub>3</sub>O<sub>4</sub>-B interface model is the most stable one in the whole allowed range and the Au-A/Fe<sub>3</sub>O<sub>4</sub>-A model is the least favorable of the proposed four models. At the same time, the results of the total DOS, the spin MM, and the total energies for the four interface structures predict that the half-metallic property of bulk Fe<sub>3</sub>O<sub>4</sub> is destroyed in the Au/Fe<sub>3</sub>O<sub>4</sub> interface. However, the ferrimagnetic property remains in the relaxed Au-A/Fe<sub>3</sub>O<sub>4</sub>-A and Au-B/Fe<sub>3</sub>O<sub>4</sub>-A structures but is destroyed in the relaxed Au-A/Fe<sub>3</sub>O<sub>4</sub>-B and Au-B/Fe<sub>3</sub>O<sub>4</sub>-B structures, which show FM ground states. This paper presents a detailed theoretical study on Au(100)/Fe<sub>3</sub>O<sub>4</sub>(100) interface.



(a) Au-B/Fe<sub>3</sub>O<sub>4</sub>-A relaxed model

FIG. 6. (Color online) Layer-projected DOS of the relaxed (a) Au-B/Fe<sub>3</sub>O<sub>4</sub>-A model, (b) Au-A/Fe<sub>3</sub>O<sub>4</sub>-B model, and (c) Au-B/Fe<sub>3</sub>O<sub>4</sub>-B model (black solid curves, spin-up states; red dashed curves, spin-down states; and dotted curves, the Fermi level).

#### ACKNOWLEDGMENTS

This work was supported by the National Natural Science Foundation of China under Grant Nos. 10574047, 10574048, and 20490210. It was also supported by National 973 project under Grant No. 2006CB921600.

\*FAX: +86 27 87544525. Electronic address: liyanli128@163.com

†FAX: +86 27 87544525. Electronic address: klyao@hust.edu.cn

<sup>1</sup>H.-J. Kim, J.-H. Park, and E. Vescovo, Phys. Rev. B **61**, 15284 (2000).

<sup>2</sup>K. Nagao, J. B. Neaton, and N. W. Ashcroft, Phys. Rev. B **68**, 125403 (2003).

<sup>3</sup>S. van Dijken, X. Fain, S. M. Watts, and J. M. D. Coey, Phys. Rev. B **70**, 052409 (2004).

<sup>4</sup>E. Snoeck, C. Gatel, R. Serra, G. Ben Assayag, J. B. Moussy, A. M. Bataille, M. Pannetier, and M. Gautier-Soyer, Phys. Rev. B **73**, 104434 (2006).

<sup>5</sup>F. Schedin, L. Hewitt, P. Morrall, V. N. Petrov, G. Thornton, S. Case, M. F. Thomas, and V. M. Uzdin, Phys. Rev. B **58**, R11861 (1998).

<sup>6</sup>G. A. Prinz, Science **282**, 1660 (1998).

<sup>7</sup>S. A. Wolf, D. D. Awschalom, R. A. Buhrman, J. M. Daughton, S.

V. Molnar, M. L. Roukes, A. Y. Chtchelkanova, and D. M. Treger, Science **294**, 1488 (2001).

<sup>8</sup>J. Feng, W. Q. Zhang, and W. Jiang, Phys. Rev. B **72**, 115423 (2005).

<sup>9</sup>C. Cheng, Phys. Rev. B **71**, 052401 (2005).

<sup>10</sup>L. Néel, Ann. Phys. **3**, 137 (1948).

<sup>11</sup>T. A. Sorenson, S. A. Morton, G. D. Waddill, and J. A. Switzer, J. Am. Chem. Soc. **124**, 7604 (2002).

<sup>12</sup>J. M. Gaines, P. J. H. Bloemen, J. T. Kohlhepp, C. W. T. Bulle-Lieuwma, R. M. Wolf, A. Reinders, R. M. Jungblut, P. A. A. van der Heijden, J. T. W. M. van Eemeren, J. aan de Stegge, and W. J. M. de Jonge, Surf. Sci. **373**, 85 (1997).

<sup>13</sup>S. A. Chambers, S. Thevuthasan, and S. A. Joyce, Surf. Sci. **450**, L273 (2000).

<sup>14</sup>A. V. Mijiritskii and D. O. Boerma, Surf. Sci. **486**, 73 (2001).

<sup>15</sup>B. Stanka, W. Hebenstreit, U. Diebold, and S. A. Chambers, Surf.

- Sci. **448**, 49 (2000).
- <sup>16</sup>F. C. Voogt, T. Fujii, P. J. M. Smulders, L. Niesen, M. A. James, and T. Hibma, Phys. Rev. B **60**, 11193 (1999).
- <sup>17</sup>R. Pentcheva, F. Wendler, H. L. Meyerheim, W. Moritz, N. Jedrecy, and M. Scheffler, Phys. Rev. Lett. **94**, 126101 (2005).
- <sup>18</sup>L. A. Kalev, P. Schurer, and L. Niesen, Phys. Rev. B **68**, 165407 (2003).
- <sup>19</sup>G. Mariotto, S. Murphy, and I. V. Shvets, Phys. Rev. B **66**, 245426 (2002).
- <sup>20</sup>M. L. Rudee, D. J. Smith, and D. T. Margulies, Phys. Rev. B **59**, R11633 (1999).
- <sup>21</sup>P. Blaha, K. Schwarz, G. K. H. Madsen, D. Kvasnicka, J. Luitz, WIEN2K, Vienna University of Technology, 2002, improved and updated UNIX version of the original copyrighted WIENCODE, which was published by P. Blaha, K. Schwarz, P. Sorantin, and S. B. Trickey, Comput. Phys. Commun. **59**, 399 (1990).
- <sup>22</sup>X. G. Wang, W. Weiss, S. K. Shaikhutdinov, M. Ritter, M. Petersen, F. Wagner, R. Schlogl, and M. Scheffler, Phys. Rev. Lett. **81**, 1038 (1998).
- <sup>23</sup>V. I. Anisimov, I. S. Elfimov, N. Hamada, and K. Terakura, Phys. Rev. B **54**, 4387 (1996).
- <sup>24</sup>V. N. Antonov, B. N. Harmon, V. P. Antropov, A. Ya. Perlov, and A. N. Yaresko, Phys. Rev. B **64**, 134410 (2001).
- <sup>25</sup>D. J. Huang, C. F. Chang, H.-T. Jeng, G. Y. Guo, H.-J. Lin, W. B. Wu, H. C. Ku, A. Fujimori, Y. Takahashi, and C. T. Chen, Phys. Rev. Lett. **93**, 077204 (2004).
- <sup>26</sup>W. Hamilton, Phys. Rev. **110**, 1050 (1958).
- <sup>27</sup>R. W. G. Wyckoff, *Crystal Structures*, 2nd ed. (Interscience, New York, 1964).
- <sup>28</sup>H. Yu, M. Chen, P. M. Rice, S. X. Wang, R. L. White, and S. H. Sun, Nano Lett. **5**, 379 (2005).
- <sup>29</sup>C. A. Ventrice, Jr., Th. Bertrams, H. Hannemann, A. Brodde, and H. Neddermeyer, Phys. Rev. B **49**, 5773 (1994).
- <sup>30</sup>C. Noguera, J. Phys.: Condens. Matter **12**, R367 (2000).
- <sup>31</sup>J. C. Boettger, Phys. Rev. B **49**, 16798 (1994).
- <sup>32</sup>V. Fiorentini and M. Methfessel, J. Phys.: Condens. Matter **8**, 6525 (1996).
- <sup>33</sup>I. G. Batyrev, A. Alavi, and M. W. Finnis, Phys. Rev. B **62**, 4698 (2000).
- <sup>34</sup>J. Rogal, K. Reuter, and M. Scheffler, Phys. Rev. B **69**, 075421 (2004).
- <sup>35</sup>Y. J. Kim, C. Westphal, R. X. Ynzunza, H. C. Galloway, M. B. Salmeron, M. A. Van Hove, and C. S. Fadley, Phys. Rev. B **55**, R13448 (1997).